Silica-coated magnetic nanorods with zwitterionic surface functionalization to overcome non-specific protein adsorption

Sirine El Mousli, Yvonne Dorant, Enzo Bertuit, Emilie Secret, Jean-Michel Siaugue

Silica-coated magnetic nanorods with zwitterionic surface functionalization to overcome non-specific protein adsorption

Sirine El Mousli, Yvonne Dorant, Enzo Bertuit, Emilie Secret* and Jean-Michel Siaugue*

Sorbonne Université, CNRS, PHysico-chimie des Électrolytes et Nanosystèmes InterfaciauX (PHENIX), F-75005 Paris, France.

E-mail: emilie.secret@sorbonne-universite.fr, jean-michel.siaugue@sorbonne-universite.fr

Abstract

Anisotropic magnetic nanoparticles are receiving growing interest for biomedical applications due to their interesting properties, particularly for MRI and magnetic hyperthermia. In this work, a two-step, relatively simple synthesis pathway of magnetite nanorods was optimised. A ligand from the catechol family, known for its high iron oxide surface affinity, was used to transfer them into aqueous phase. The magnetite nanorods were then coated with a layer of fluorescent silica, whose surface was functionalised in two ways: either by short poly(ethylene glycol) (PEG) chains or by sulfobetaine zwitterionic molecules. A wide range of techniques were used to thoroughly characterise their physical structure, magnetic properties and dispersion characteristics. Finally, a study of the adsorption of a fluorescent model protein revealed that zwitterionic sulfobetaine molecules were more effective than PEG chains in limiting the non-specific adsorption of this protein.

Keywords : magnetite, nanorods, silica, zwitterionic coating, PEG coating, nonfouling.

1. Introduction

Nanoparticles (NPs), and especially magnetic nanoparticles (MNPs), are widely studied for biomedical applications such as imaging, drug delivery, hyperthermia, cellular engineering or biosensing[1]. In the vast majority of studies, the NPs or MNPs used are spherical. However, new shapes of NPs have arisen due to their particular properties, such as nanocubes, nanoflowers, nanotriangles, nanorods (NR), nanowires (NW), nanotubes (NT), nanostars or nano-urchins. Nanochains (NC), obtained by pre-assembling spherical MNPs, which are then coated with a layer of silica, are another example of recently developed anisotropic MNPs[2]. In particular, elongated NPs, such as NR, NW, NT or NC are of utmost interest for biomedical applications, because of the interesting properties that their shapes lead to. For example, elongated NPs have been shown to exhibit a longer circulation time *in vivo*, a better biodistribution and a longer retention time inside the tumour compared to their spherical counterparts[3]–[5]. Functionalizing elongated NPs with antibodies lead to an enhancement of the specific recognition of their target and a decrease of the non-specific recognition, compared to spherical NPs[6]. Nanostructures, with a bundle-like morphology, synthesised from magnetic NCs and exhibiting high transverse relaxivity, have also been described[7]. Thanks to the possibility to have multiple interactions between NRs and cellular receptors, NRs can be more efficiently fixed to cancer cells. The elongated shape of NPs can also have an effect on the protein corona surrounding them. If NRs can adsorb more proteins on their surface than nanospheres, the denaturation rate of these adsorbed proteins is higher on the sphere than on the rods[8]–[10]. The high aspect ratio of NRs also has an impact on their cellular internalization. For example, high aspect ratio gold NRs showed an increased cellular internalization compared to NPs with lower aspect ratio[11]. It was also shown that some type of elongated NPs, such as carbon[12], [13] or titanate NTs[14] were able to by-pass the endocytosis pathway to passively diffuse across the cellular membrane, and hence reach the cytosol, which could enable the targeting of intracellular proteins or organelles. Finally, it was demonstrated that magnetic NRs displayed higher r_2 relaxivities in MRI[15] and better heating efficiency in magnetic hyperthermia[16], [17] than their spherical counterparts. All these properties taken together make magnetic NRs excellent candidates for biomedical applications.

Several groups already tried to optimize and rationalize the magnetite NRs syntheses and different synthesis methods of such NRs have been already presented in the literature. Magnetite NRs can be obtained in one step by co-precipitation with Dextran® as a templating agent[18], or by inverse co-precipitation under a magnetic field[19]. NRs with lengths ranging from 60 to 140 nm can also be obtained by a solvothermal synthesis with $Fe(CO)_5$, oleic

acid and hexadecylamine[20]. A high-temperature synthesis protocol using a previously prepared iron oleate complex as a precursor was also reported[21]. Nevertheless, the most studied processes to synthesize magnetite NRs rely on two steps, where non-magnetic iron oxide NRs are firstly synthesized and then reduced to obtain magnetite NRs.

In particular, one of these two-step syntheses was chosen in the present study for its supposed simplicity of execution, compared for example to synthesis where NPs are calcinated under H_2 at 450°C[22], for the low cost of the chemicals used and for the morphology of the obtained NRs that were suited for biomedical applications[15]. This synthesis is based on the formation of akaganeite (β-FeOOH) NRs with poly(ethylene imine) as a templating agent, followed by their reduction into magnetite using oleylamine as a solvent and a reducing agent. While the reduction of akaganeite to magnetite by oleylamine leads to a decrease in the size of the NRs, the overall anisotropic shape is maintained. The control of the reduction process is an important step, since akaganeite nanorods have also already been used as precursors in the synthesis of other types of iron oxide, notably metastable phases such as ε-Fe_2O_3, by annealing with precise temperature control[23], [24].

However, many practical issues were encountered when trying to replicate this synthesis, due to a lack of details in studies reported in the literature. An optimization of the process was thus carried out by varying parameters such as the concentration of the precursor salts used (ferric chloride) and of the templating agent, or the reducing conditions. A protocol for aqueous phase transfer of the synthesized NRs was then developed based on the previous work of Liu *et al*[25]. A thorough characterization of the synthesized NRs was then performed.

To be used in biomedical applications, NPs need to be colloidally stable and to be able to be functionalised with biomolecules. The aggregation of NPs leads to an increase in their size, which modifies their biodistribution *in vivo*, reduces their circulation time and finally leads to their elimination by the reticulo-endothelial system. Depending on their surface functionalisation, NPs can be colloidally stabilised in water thanks to repulsive, electrostatic and steric forces, in order to limit their aggregation[1]. For these reasons, the obtained NRs were here coated by a silica shell, as the silica layer makes possible both to contain fluorophores necessary for *in vitro* monitoring and to further functionalize the surface of the NR with biomolecules and stability agents. In this study, the magnetic silica coated NRs were functionalised either with short polyethylene glycol (PEG) chains or with sulfobetaine zwitterionic molecules in order to compare their protein adsorption capacity. Indeed, particular attention needs to be paid to the events occurring when the NPs are in contact with a biological medium, as it contains proteins, sugars *etc*. which form a protein corona surrounding the NPs. While PEG remains the gold standard in nanomedicine to make stealth NPs, in the last few years zwitterionic molecules were shown to induce a low non-specific protein adsorption at the surface of NPs[26]–[28]. They can thus avoid quick recognition by the immune system and exhibit delayed blood clearance from the body, making them promising candidates in nanomedicine.

We thus report in this article the synthesis of silica coated magnetite nanorods functionalized either with short PEG chains or with sulfobetaine zwitterionic molecules. Their physical structure, magnetic properties and dispersion properties were characterised using a wide range of techniques. A protein adsorption quantification was also conducted and revealed that zwitterionic surface functionalization is more efficient than short PEG chains to impede non-specific adsorption of proteins.

2. Experimental section

2.1 Materials

30% ammonia, sodium hydroxide, acetone, ethanol, hexane, tetrahydrofuran and iron(III) chloride hexahydrate ($FeCl_3 \cdot 6H_2O$) were purchased from VWR chemicals (Radnor, USA). 3-(N-morpholino)propanesulfonic acid sodium salt (MOPS), linear poly(ethyleneimine) (PEI) (M_w = 5000 g/mol), 70 % oleylamine, 3,4-dihydroxyhydrocinnamic acid (DHCA), tetraethyl-orthosilicate (TEOS), 3-aminopropyltriethoxysilane (APTS), rhodamine B isothiocyanate (RITC) and polyacrylic acid (PAA) (M_w = 2100 g/mol) were purchased from Sigma Aldrich (Darmstadt Germany). 90% 3-[methoxy(polyethylenoxy)]propyltrimethoxysilane (PEOS) was purchased from ABCR (Karlsruhe, Germany). 3-[dimethyl(3-trimethoxysilyl)propyl]ammonio propane-1-sulfonate (ZSSi) was purchased from Gelest (Morrisville, PA, USA). Dulbecco's modified Eagle's-F12 medium (DMEM-F12), penicillin, streptomycin, and trypsin were purchased from Gibco (France). All reagents were used without further purification. Distilled water was used for all experiments.

2.2 Synthesis of akaganeite nanorods (β-FeOOH)

A defined amount of $FeCl_3$-6(H_2O) was dissolved in 100 mL of water. As a mean of size control, PEI was added in different quantities. The PEI used had a molecular weight of 5000 g/mol and was linear. The mixture was heated at 80°C for 2 hours under magnetic stirring and under a nitrogen atmosphere. The solution was then cooled down to

room temperature and centrifuged for 20 minutes at 10,000 rpm. The obtained NRs were washed three times with an ethanol/water solution (1/1 v/v) and finally dispersed in water.

2.3 Synthesis of magnetite nanorods (Fe_3O_4)

500 mg of centrifuged akaganeite NRs were mixed with 8 mL of oleylamine (25 mmol). To fully disperse the particles in oleylamine, they were vortexed and placed in an ultrasonication bath for 15 minutes. The solution was then heated at 200°C for 4 hours, without magnetic stirring, the solution being stirred by nitrogen bubbling. The brownish solution turned black. The obtained NRs were washed twice with a hexane/acetone solution (1/1 v/v) and finally dispersed in hexane.

2.4 Phase transfer of the magnetite NRs

In order to transfer the magnetite NRs from hexane to water, ligand exchange between oleylamine and DHCA was performed. 50 mg (0.28 mmoles) of DHCA were dissolved in 6 mL of tetrahydrofuran and then heated to 50°C. 1 mL of the dispersion of NRs in hexane was then added and the resulting solution was heated for 3 hours at 50°C. 500 µL of a solution of sodium hydroxide (0.5 M) was then added to precipitate the particles. The particles were magnetically separated from the solution and finally dispersed in water.

2.5 Synthesis of silica coated magnetite nanorods (Fe_3O_4@SiO_2)

In order to coat the magnetite nanorods with silica, a pre-functionalization step using PAA was required. 10 mL of an aqueous solution of magnetite NRs (10 mg/mL) was stirred overnight with an equal volume of an aqueous solution of PAA (0.1 g/mL). The PAA excess was removed by washing the NRs three times with water. The obtained NRs were dispersed in 30 mL of water. The silica coating was then performed as follows: 4 mL of the aqueous solution of magnetite NRs, 0.8 mL of a 30 % ammonia solution and 14 mL of ethanol were first mixed in a vial by vigorous stirring, followed by the addition of 40 µL (0.18 mmoles) of TEOS. After 1 hour of reaction, the NRs were washed twice with water and redispersed in 5 mL in a water/ethanol solution (1/2 v/v). For PEG or sulfobetaine surface functionalization, 25 µL (0.046 mmoles) of PEOS or 125 µL of an aqueous solution of ZSSi (0.1 g/mL, 0.038 mmoles), as well as 13 µL of RITC-APTS previously prepared (10 mg of RITC, 1 mL of EtOH and 9 µL of APTS left to react overnight) were added to the dispersed NPs and left to react overnight. The obtained NPs were washed three times with water and redispersed in 5 mL of MOPS buffer.

2.6 Characterization

The morphology of synthesized NPs was characterized by transmission electron microscopy (TEM, JEOL 1011). A droplet of NPs dispersion (in water or in hexane) was deposited on a carbon-coated copper grid and air-dried at room temperature. Lengths, diameters and aspect ratios were measured using ImageJ software ($n \geq 200$) and the data obtained were analysed as the mean ± standard deviation (normal law). Scanning electronic microscopy (SEM) was performed on a SEM-FEG Hitachi SU-70.

Dry samples of NRs were analysed by X-ray diffraction on a Rigaku Ultima IV. X-ray absorption near edge spectroscopy (XANES) at Fe K-edge was performed at Synchrotron SOLEIL on the ROCK beamline in 1 mm diameter glass capillary.

The total iron concentrations of all samples were measured by atomic absorption spectroscopy (AAS, PinAAcle 500, Perkin Elmer).

The magnetic properties of the produced NRs dispersed in water were measured using Quantum Design Physical Properties Measurement System (PPMS 6500) and Superconducting Quantum Interference Device (SQUID, MPMS-XL). The magnetization curves were recorded between 0 and 20 kOe. Zero field-cooled (ZFC) and field-cooled (FC) measurements were performed over the 5–250 K temperature range. The applied field for ZFC/FC measurements was set to 50 Oe. The magnetization values have been normalised to the total mass of magnetic material in the sample.

Dynamic light scattering (DLS) and zeta-potential measurements were performed on a Malvern Zetasizer instrument.

Small angle X-ray scattering (SAXS) was performed at Synchrotron SOLEIL on the SWING beamline, in 1 mm diameter glass capillary.

2.7 Protein adsorption studies

Hydrodynamic diameter studies

Silica coated magnetite NRs, with PEG or sulfobetaine surface functionalization, were dispersed at an iron concentration of 20 mM in DMEM-F12 medium supplemented with serum and incubated at 37°C during 1 h. The

NPs where then washed 3 times with MOPS buffer and redispersed in 500 µL of MOPS buffer. The hydrodynamic diameter of the NPs was measured by DLS.

Green fluorescent protein adsorption experiments

The obtained NPs, with PEG or sulfobetaine surface functionalization, and with RITC, were dispersed at an iron concentration of 20 mM in MOPS buffer with various concentrations of green fluorescent proteins (GFP), ranging from 3 to 60 ng/mL and incubated at 37°C during 1 hour. Afterwards, the NPs were washed 3 times with MOPS buffer and redispersed in 500 µL of MOPS buffer. The fluorescence intensity of the NPs (due to the RITC) and of the adsorbed GFP were analysed by fluorescence spectroscopy with a SpectraMax i3X instrument (Molecular Devices) and the ratio [GFP adsorbed]/[Nanoparticles] was plotted against [GFP introduced].

3. Results and discussion

3.1 Synthesis of akaganeite nanorods (β-FeOOH)

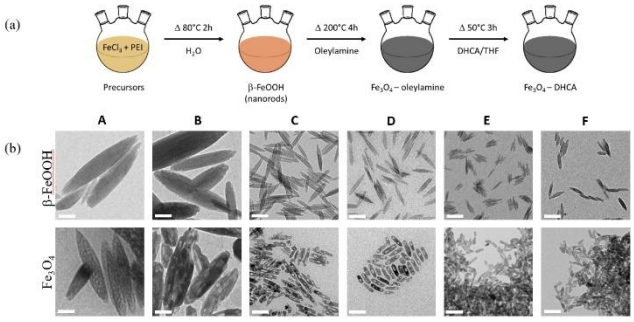

Fig. 1 (a) Two-step synthesis procedure of magnetite NRs and their subsequent transfer to an aqueous phase (b) TEM images of synthesised akaganeite and magnetite NRs according to the experimental conditions (A to F) described in Table 1. All scale bars are 50 nm.

Aqueous-phase dispersions of magnetite NRs were obtained using a two-step synthesis procedure, reported in Figure 1, followed by a phase transfer from hexane to water. In the first step of this synthesis procedure[15], [29], which is fairly simple to implement, anisotropic akaganeite NPs were synthesised in aqueous phase by heating an inexpensive and abundant iron precursor, $FeCl_3$, to 80°C for two hours, in the presence of varying amounts of PEI.

Consequently, akaganeite NPs were synthesised for two different $FeCl_3$ concentrations, in the absence and presence of PEI (linear, M_w =5000 g/mol), at two different PEI/Fe ratios for each of these two iron concentrations. The results for the size (lengths, diameters) and aspect ratio of the obtained akaganeite NPs are reported in Table 1. The corresponding histogram distributions, which are provided as supplementary material (Fig. S1 a-f), were analysed using a normal law (Fig. S1 a-f, red curves). Representative TEM images of the akaganeite NPs obtained for each experimental condition used are shown in the first line of Figure 1b.

	[Fe]/ [PEI]	[PEI] (mol/l)	[$FeCl_3$] (mol/L)	Length (nm)	Diameter (nm)	Aspect ratio
A	∞	0	0.2	*182 ± 68*	*31 ± 13*	5.8 ± 0,9
B	∞	0	0.1	*154 ± 66*	*35 ± 13*	4.3 ± 1,0
C	1000	0.0002	0.2	64 ± 16	11 ± 2	5.9 ± 1,0
D	1000	0.0001	0.1	59 ± 10	12 ± 2	5.0 ± 0,8
E	400	0.0005	0.2	26 ± 8	5 ± 1	4.9 ± 1,3
F	400	0.00025	0.1	35 ± 8	8 ± 2	4.5 ± 0,9

Table 1: Lengths, diameters and aspect ratios of the akaganeite NRs synthesised in this work.

In the absence of PEI (Table 1, lines A and B), anisotropic NPs with a spindle-shaped morphology are obtained. They were characterised by a very broad size distribution, which cannot be properly fitted using a normal or log-normal law. For comparison with the other samples, the mean diameters and lengths resulting from analysis of the size distribution using a normal law is shown in Table 1 (Fig S1, a-b, red curves), but analysis using a double normal law seems more relevant (Fig S1, a and b, green curves). This procedure, carried out in the absence of PEI at these two iron concentrations, therefore leads to samples containing NPs of at least two size ranges, a majority

characterised by a length of around 150-200 nm, and a minority characterised by a length of around 300-350 nm. The different sizes observed for these two batches of NPs are similar and the iron concentration therefore seems to have only a slight influence.

The addition of PEI to the reaction medium not only decreases the size of the NPs, but also gives a much narrower size distribution. Unlike the concentration of iron, the concentration of PEI enables the control of the size of the NPs. The more PEI present in the reaction medium, the smaller the obtained akaganeite nanorods get. Thus, for an iron concentration of 0.2 mol/L, the length and diameter of the NPs are respectively 64 and 11 nm for an Fe/PEI ratio of 1000 (Table 1, row C) and 26 and 5 nm for an Fe/PEI ratio of 400 (Table 1, row E). The same trend was observed for an iron concentration of 0.1 mol/L (Table 1, lines D and F) with similar sizes, confirming the predominant influence of the proportion of PEI on the size of the NPs, whatever the iron concentration, in the studied concentration range.

The adsorption of PEI onto the surface of the NRs is responsible for this decrease in size, as shown by several previous studies[30], [31]. Although it allows NPs growth to be limited, it does not allow a preferential orientation along the longitudinal axis, as shown by the aspect ratios which are of the same order of magnitude for all the samples, with or without PEI.

3.2 Synthesis of magnetite nanorods (Fe_3O_4)

The second step of the synthesis procedure consists in the reduction of akaganeite to magnetite, with some of iron(III) ions being reduced to iron(II) ions. The akageneite NRs are dispersed in oleylamine and heated at 200°C for 4h, according to a previously described procedure[15], [29]. The oleylamine acts as a solvent, both reducing and capping agent, preventing the NPs from aggregating. The temperature and heating duration must be carefully controlled for this delicate step, during which the anisotropic shape of the NPs can be lost. For example, heating for 6 hours leads to the formation of spherical NPs whereas heating for 2 hours allowed only an incomplete reduction of the akaganeite NRs. (Fig. S2).

Table 2 presents the sizes (lengths, diameters) and aspect ratios for the obtained magnetite NRs, as a function of $FeCl_3$ and PEI concentrations used during the first synthesis step. The corresponding histogram distributions, which are provided as supplementary information (Fig. S3 a-f), were analysed using a normal law (Fig. S3 a-f, red curves). Representative TEM images of the magnetite NPs obtained for each experimental condition used are shown in the second line of Figure 1b.

In the absence of PEI in the first step of the synthesis, the polydispersity of the akaganeite precursors leads to the production of highly polydisperse magnetite NRs after the reduction step (Tables 1 and 2, lines A and B). Once again, analysing the size distribution is difficult. Only the use of a double normal distribution allows this distribution to be properly fitted (Fig S3, a and b, green curves), indicating the presence of NPs in two size ranges, smaller overall than before the reduction step. For comparison purposes, the mean diameters and lengths resulting from the analysis of the size distribution by a normal law are nevertheless presented in Table 1 for samples A and B (Fig S3, a-b, red curves).

	[Fe]/ [PEI]	[PEI] (mol/l)	[$FeCl_3$] (mol/L)	Length (nm)	Diameter (nm)	Aspect ratio
A	∞	0	0.2	*224 ± 72*	*49 ± 14*	4.4 ± 0,8
B	∞	0	0.1	*147 ± 69*	*44 ± 25*	3.4 ± 0,9
C	1000	0.0002	0.2	51 ± 16	12 ± 2	4.1 ± 1,1
D	1000	0.0001	0.1	37 ± 12	12 ± 2	2.9 ± 0,5
E	400	0.0005	0.2	21 ± 5	7 ± 1	2.8 ± 0,6
F	400	0.00025	0.1	23 ± 6	7 ± 2	3.1 ± 0,8

Table 2: Lengths, diameters and aspect ratios of magnetite NRs synthesised in this work.

A systematic decrease in size and aspect ratio is observed after the reduction step in oleylamine for the samples prepared with PEI. For example, for an iron concentration of 0.2 mol/L and an Fe/PEI ratio of 1000, the akaganeite NRs synthesised have an average length of 64 nm before reduction (Table 1, row C) while, after reduction, the obtained magnetite NRs have an average length of 51 nm (Table 2, row C). The aspect ratio also decreased, from 5.9 to 4.1. However, the elongated shape of the NPs remained after this reduction step. The TEM images of magnetite NRs (Fig. 1b) also reveal that the NRs appear to be hollowed. The formation of such pores has already been observed during the reduction of akaganeite to magnetite. The logical consequence of the formation of magnetite (ρ =5,2 g/cm^3) from a less dense phase (akaganeite, ρ = 3,0 g/cm^3), and the loss of mass corresponding to the transformation of akaganeite into magnetite, is a reduction in volume, estimated at 50% by Xu *et al.*[32]. The

protection of the surface by adsorbed ligands explains why these pores form inside the structure, while the NRs retain their morphology. The role of water has also been highlighted by Wu *et al.*[33] who proposed that dissolution and recrystallisation mechanisms are involved in the formation of these pores.

3.3 Aqueous phase transfer of the magnetite nanorods

The dispersions obtained in hexane after the reduction step were not very stable and the NRs tended to aggregate and sediment. For this reason, it was decided to transfer them to water. This third step in the synthesis procedure (Fig. 1a) led to a colloidally-stable suspension of NPs in the aqueous phase. To do so, DHCA[25], a ligand from the catechol family, well known for its high affinity for the iron oxide surface[34], [35], was used. This affinity had to be strong enough to displace the oleylamine adsorbed on the surface during the reduction step. The use of this ligand is particularly advantageous, as it is soluble in THF, which allows ligand exchange to take place on the surface of NPs in the organic phase. Then, following the addition of an alkaline reagent, deprotonation of the carboxylic acid functions leads to a highly negatively charged surface, which causes the NPs to precipitate. After magnetic separation, NPs can be redispersed in water, with repulsive electrostatic interactions ensuring the stability of the dispersion.

3.4 Synthesis of silica coated magnetite nanorods (Fe_3O_4@SiO_2)

The surface coating of magnetic NPs with a layer of silica allows functional groups (NH_2, SH, *etc*.) and polymer chains (such as PEG) to be easily introduced by the condensation of commercial organosilanes. In addition, the silica layer can be doped with a fluorophore, allowing fluorescence and magnetic properties to be combined in the NPs**.**

A first attempt to coat DHCA-functionalised magnetic NRs with a silica layer using a protocol developed by our group[36], and widely used with citrated spherical magnetic NPs[37], was unsuccessful. This protocol, inspired by the pioneering work of Stöber *et al.*[38] involves the hydrolysis and condensation of organosilanes in an alcoholic medium in the presence of ammonia. The particles obtained using this protocol were larger than the original magnetite NRs, due to the coating of large aggregates of NRz embedded in a layer of silica.

To achieve a more individual coating of the NRs, the magnetite NRs were first pre-functionalised with PAA. The increased number of carboxylic acid functions on the surface of the NPs, provided by PAA, compared to DHCA, probably improves the stability of the NPs in the synthesis medium and thus favours a more individual coating of NPs. Moreover, the carboxylic acid functions of the polymer on the surface of the NPs can also be involved in the condensation reactions, thereby promoting the growth of the silica layer onto the surface of the NPs. This modified protocol enabled NRs to be coated with a layer of silica without observing a dramatic increase in the size of the NRs. (Figure 2).

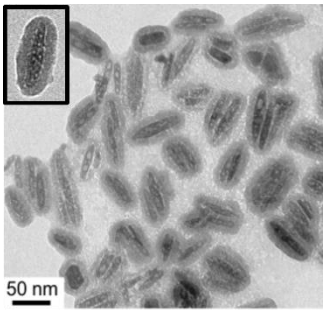

Fig. 2 Representative TEM image of magnetite DHCA-functionalised NRs coated with a silica layer.

The first step in the coating protocol consists in the hydrolysis and condensation of TEOS to form the silica layer (NR@SiO_2). The second step involves the functionalisation of the silica surface by functionalised organosilanes. To compare their contribution in terms of colloidal stabilisation and reduction of protein adsorption, two organosilanes were used, one functionalised by a short PEG chain (NR@SiO_2-PEG) and the other by a zwitterionic sulfobetaine molecule (NR@SiO_2-ZSSi)[28]. Both of them were also functionalised with rhodamine B, in order to obtain fluorescent magnetic NRs[39].

3.5 Characterization

From now on, all the results presented and discussed will be related to sample D, which was chosen because its morphology is the most suitable one for the future biomedical applications envisioned.

Akaganeite and magnetite NPs were characterised by X-ray powder diffraction (Figure 3A). The diffractogram obtained for the akaganeite NPs shows three characteristic peaks associated with the (3 1 0), (2 1 1) and (5 2 1) planes (ICDD Card No. 34-1266), while the one obtained for the magnetite NPs corresponds well to the expected spinel structure, with six diffraction

peaks for (2 2 0), (3 1 1), (4 0 0), (4 2 2), (5 1 1) and (4 4 0) planes representing the face centred cubic structure (ICDD Card No.72-8151). These two diffractograms confirm that akaganeite NPs were obtained during the first step and that akaganeite was reduced into magnetite during the second reduction step.

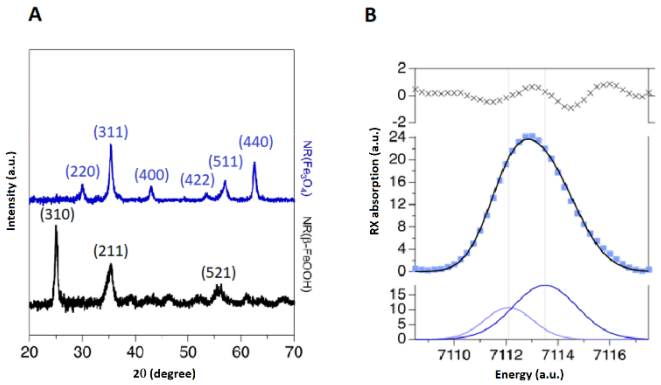

Fig. 3 A) XRD diffractograms of akaganeite (NR(β-FeOOH), black line) and magnetite (NR(Fe_3O_4), blue line) NRs. B) XANES analysis of magnetite NRs (squares: experimental points; black curve: double normal law fit; black crosses: residues; light blue curve: contribution of Fe(II), dark blue curve : contribution of Fe(III)).

The lattice parameter a of the face-centred cubic spinel structure of magnetite NRs was determined according to equation (1):

$$\mathbf{a} = \frac{\lambda_{Cu}}{2\sin(\theta_{hkl})}\sqrt{\mathbf{h^2 + k^2 + l^2}} \qquad (1)$$

where λ_{Cu} is the wavelength of the copper K_α X-ray source (1.54 Å), θ_{hkl} is the diffraction angle and h, k, l are the Miller indexes of the crystalline planes.

A value of 8.387 ± 0.011 Å was thus obtained, in perfect agreement with the value of 8.390 Å expected.

The physical diameter of the magnetite NRs was then determined using the Scherrer equation (2):

$$\mathbf{d} = \frac{0{,}89\lambda_{Cu}}{\beta\cos\theta} \qquad (2)$$

where β is the full-width at half-maximum of the considered diffraction peak.

A diameter of 11 ± 1 nm was thus calculated, which is consistent with the average diameter of 12 ± 2 nm for sample D determined by size analysis using TEM micrographs.

In order to obtain a quantification of the stoichiometry of the magnetite samples, XANES at Fe K-edge analyses were carried out (Figure 3B). After correcting[40] and normalising[41] the data, the pre-peak is modelled by the deconvolution of two Gaussians centred at 7112.1 eV and 7113.5 eV, corresponding to the contributions of Fe(II) and Fe(III) ions respectively[42]. The ratio Fe(II)/Fe(III) is determined by the area ratio of each contribution and was equal 0.46, very close to the theoretical ratio of 0.5 expected for magnetite. The small discrepancy corresponds to the existence of an oxidised maghemite surface layer, but of very small thickness, estimated at approximately 0.3 nm.

A high-resolution TEM study (Figure 4) was also performed on the magnetite NRs to characterise their crystalline structure. The high-resolution micrograph shows regularly paralleled lattice fringes indicating a monocrystalline structure, confirmed by the single dots on the Fourier transform (FT) pattern of the selected area (insert in Figure 4). The magnetite NRs are therefore single-crystals despite the porosity observed in the structure, meaning that pores do not prevent the continuity and alignment of the crystal planes. Moreover, the HR-TEM image reveals that the inter-plane distance is equal to 0.3 nm, which corresponds to the (2 2 0) crystal plane of the magnetite[43], [44].

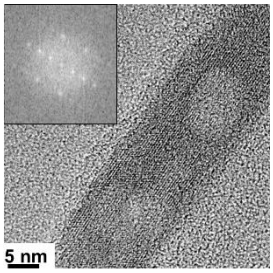

Fig. 4 HR-TEM image of a magnetite NR. Insert: Fourier transform of the selected area.

Figure 5A shows the magnetisation curves as a function of the applied magnetic field over the temperature range 5-250 K. Saturation magnetisation varies from 21 emu/g at 5 K to 15 emu/g at 250 K. Several factors are responsible for these much lower saturation magnetization values than expected for bulk magnetite (92 emu/g). The 0.3 nm oxidised maghemite surface layer is not large enough to explain this magnetisation value. Indeed, it corresponds to a maghemite mass proportion of only about 5.6%. Its contribution to the reduction of the saturation magnetisation of NRs in comparison with that of bulk magnetite is therefore very low. However, for such small sizes, characterised by a high surface-to-volume ratio, the phenomenon of spin canting, *i.e.* the existence of a surface spin disorder layer, is probably responsible for a significant decrease in saturation magnetisation. Mohapatra *et al.* showed that the thickness of this layer could be determined from the difference with the magnetisation saturation of the bulk material and that this thickness decreased as the size of the NPs increased[45]. However, in our case, such an estimation is not straightforward, because of the anisotropic shape of NRs and especially of their porosity, which necessarily modifies the surface/volume ratio. The shape anisotropy of NRs may also be involved, since it has already been shown for NRs that increasing the aspect ratio leads to a decrease in saturation magnetisation[46]. Indeed, the high values of coercivity observed, from 470 Oe at 5 K to 150 Oe at 250 K, reveal the existence of an easy axis of magnetization parallel to the NR axis[47]. An increase in the coercive field with aspect ratio was also demonstrated, by comparing the magnetic properties of spherical MNPs and anisotropic MNPs. In fact, the trend towards orientation along this easy magnetic axis rather than along the field direction, lowering the saturation magnetization, increases with the aspect ratio, *i.e*. the shape anisotropy[48]. Such behaviour demonstrates that the shape anisotropy has a strong influence on the magnetic properties of NRs.

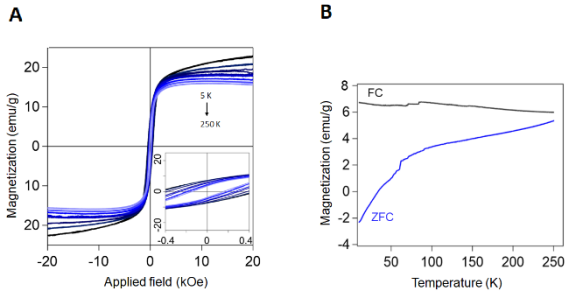

Fig. 5 A) Magnetisation curves as a function of the applied magnetic field over the temperature range 5-250 K B) Field-cooled (FC) and zero field-cooled (ZFC) magnetization curves.

Field-cooled (FC) and zero field-cooled (ZFC) magnetization curves are reported in the figure 5B. No blocking temperature is observed, confirming that the NRs are magnetically blocked in the studied temperature range (5-250 K). The Verwey transition is not clearly observed on the ZFC curve, probably because the NRs are too small. Indeed, it has already been reported that this transition weakens as the size of the NRs decreases, with a higher surface-to-volume ratio resulting in higher spin surface disorder[46]. The absence of this transition for small nanoparticles may also be due to surface oxidation. Indeed, It has been reported that the Verwey transition was not observed for nanoparticles containing even a very small proportion of maghemite[49]. It has been shown that this transition disappears when the off-stoichiometry parameter δ, defined as $Fe_3(1-\delta)O_4$, is larger than 1%[50], [51]. The mass percentage of maghemite, deduced from the Fe(II)/Fe(III) ratio of 0.46, is equal to 5.6%, giving a δ value of 0.68%. Thus, surface oxidation alone cannot explain the disappearance of the Verwey transition. It may therefore be due to a combination of the two factors, spin canting and surface oxidation, as previously reported for small spherical MNPs by Mitra *et al.*[52].

At 300 K, the magnetisation tends to saturate at 14 emu/g and no notable coercivity is observed, indicating that the NRs behave as superparamagnetic NPs at room temperature. As expected for superparamagnetic NPs, zero remanent magnetisation is also observed at room temperature, which is of significant importance for biomedical applications. Indeed,

a remanent magnetisation would lead to attractive forces between the MNPs. These must be counterbalanced by repulsive forces, of a steric or electrostatic nature, to avoid aggregation, which is not always possible if the remanent magnetisation is too high[53].

The hydrodynamic diameter, measured by DLS, of the magnetite NRs at different steps of their functionalization is reported in Table 3, as well as the polydispersity index. After synthesis and transfer to the aqueous phase, the hydrodynamic diameter remains below 100 nm, which seems to be in agreement with the sizes measured by TEM. Pre-functionalisation with PAA resulted in a slight increase in hydrodynamic diameter, due to the polymer chains on the surface of the NRs. Interestingly, the polydispersity index decreased after the ligand exchange from DHCA to PAA, probably due to a better dispersion of the NRs in water. On the contrary, coating with silica results in a sharp increase in hydrodynamic diameter, as well as an increase in the polydispersity index. This indicates the presence of larger particles corresponding to small aggregates obtained by the coating of several NRs into the same silica shell, as well as single NRs coated with silica. This result is in perfect agreement with the previous observation made from TEM image (Figure 2).

	Hydrodynamic diameter (nm)	Polydispersity index
NR@DHCA	88	0.21
NR@PAA	102	0.12
NR@SiO_2	207	0.38
NR@SiO_2-PEG	284	0.25
NR@SiO_2-ZSSi	216	0.34

Table 3: Hydrodynamic diameters and polydispersity indexes of magnetite NRs synthesised in this work.

The study of the surface charge, by measuring the zeta potential, as a function of pH is shown in Figure 6A. The negative surface charge observed for magnetite NRs coated by a layer of non-functionalised silica (NR@SiO_2), which is very high at high pH values, corresponds to the deprotonation of the silanol functions (Si-OH = Si-O^- + H^+) on the surface of the silica layer. The progressive protonation of these functions leads to an increase in the zeta potential as the pH decreases, to a near-zero value at pH 2, close to the point of zero charge of silica. The same trend is observed for magnetite NRs covered by a layer of silica functionalised by PEG chains (NR@SiO_2-PEG). This proves that the silica surface, characterised by the type and approximate proportion of silanol functions (isolated, geminal and vicinal)[54], with different acidity constants, is similar for these two types of NPs. In opposition, magnetite NRs covered by a layer of silica functionalised by sulfobetaine molecules (NR@SiO_2-ZSSi) behave very differently, since the zeta potential scarcely changes with the pH. As the sulfobetaine molecules are neutral overall, since they contain a quaternary ammonium function and a sulfonate function, the negative surface charge is due to the deprotonation of some of the silanol functions. Such a trend has already been observed for silica NPs functionalised with the same zwitterionic organosilane. However, in this previous work, the zeta potential was close to zero whatever the pH. A very significant cross-linking of the silica layer, induced by a heating step, leading to the almost complete disappearance of the silanol functions on the surface, was proposed to explain this evolution as a function of pH[27]. In our case, the most plausible explanation would be that the surface is strongly cross-linked and that only certain very acidic silanol functions, of a geminal (pKa = 2.9) or vicinal (pKa = 2.1) nature[55], remain. These residual silanol functions, protonated at very acidic pH, would explain this zeta potential, less negative than for non-functionalised silica at pH 7, but more or less constant up to pH 2.

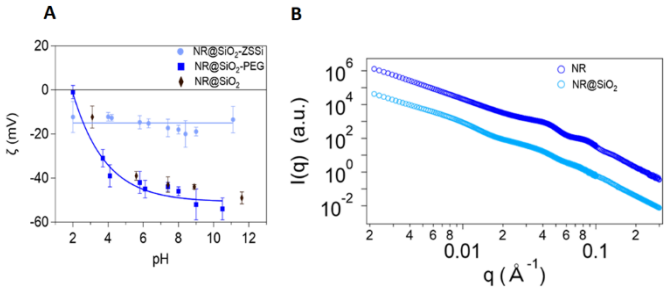

Fig. 6 A) Zeta potential as a function of pH of magnetite NRs coated by silica (NR@SiO_2, black diamonds), and further functionalised with PEG chains (NR@SiO_2-PEG, dark blue squares) or with sulfobetaine molecules (NR@SiO_2-ZSSi, light blue circles). Solid curves are only a guide for the eye. B) SAXS spectra of magnetite NR (NR, dark blue) and of magnetite NR coated by silica (NR@SiO_2, light blue).

A small-angle X-ray scattering (SAXS) study was also carried out to elucidate the structure of the NRs in solution both before and after the silica coating (Figure 6B). Similar results were obtained for both types of particles. At low values of q, the non-zero slope of the curve indicates that some of the NRs are interacting, hence a partial state of aggregation of the NRs in solution. At medium q values, the slope measured is intermediate between q^{-2} (characteristic of lamellar particles) and q^{-3} (characteristic of more complex structures), and not proportional to q^{-1} as expected for cylindrical nanorods.

To get a deeper insight of the shape of the NRs, before the silica coating, scanning electronic microscopy (SEM) was performed on NRs functionalised with DHCA (Figure 7). SEM enables objects to be viewed in three dimensions, so they can be observed from the front as well as in side, contrary to TEM. Side views revealed that the thicknesses of the NRs seem to be different from their diameters, *i.e.* that three dimensions could be needed to describe them: length, diameter and thickness. Further studies would therefore be necessary to elucidate the real shape of these nanostructures.

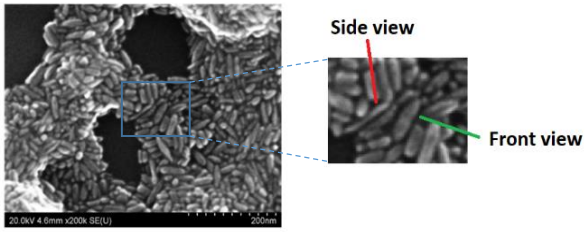

Fig. 7 Scanning electron microscopy image of magnetic NRs.

3.6 Protein adsorption studies

Preventing protein adsorption is one of the greatest challenges facing the use of magnetic NPs for biomedical applications[26], [56]. In this context, the silica shell surface of the coated magnetic NRs (NR@SiO_2) was functionalised either by short PEG chains (NR@SiO_2-PEG) or by zwitterionic sulfobetaine molecules (NR@SiO_2-ZSSi), both well known to limit protein adsorption thanks to their strong hydration layer[57]. Although the interactions with the water molecules are of different nature, the same mechanism explains their resistance to protein adsorption. The interactions with the water molecules on the surface, by hydrogen bonding in the case of PEG chains[58] and by electrostatic interactions in the case of sulfobetaine molecules[59], [60], prevent the displacement of the water molecules bound to the surface and subsequently the adsorption of proteins. While these two types of surface functionalisation are widely studied, only a few comparative studies of protein adsorption on the surface of similar NPs can be found[61] and none, to the best of our knowledge, about magnetic NPs.

A preliminary study consisted in evaluating the stability of the two types of NPs in a cell culture medium by DLS. No aggregation was observed after dispersion of the NPs in the culture medium. The hydrodynamic diameters measured are of the same order of magnitude as those reported in Table 3, *i.e.* approximately 220 nm for NR@SiO_2-ZSSi and 280 nm for NR@SiO_2-PEG. After one hour of incubation at 37°C in the culture medium, no significant change in hydrodynamic diameter was measured, confirming the good colloidal stability of these NPs in cell culture medium.

Next, the adsorption of a fluorescent model protein (GFP) was studied using rhodamine-fluorescent NRs. The use of fluorescent NPs enables the quantity of protein adsorbed to be standardised to the quantity of NPs effectively present in the sample. Indeed, washing steps, during which losses of NPs may occur, are required to eliminate proteins not bound to the surface after incubation. Thus, Figure 8 shows the ratio between the concentration of adsorbed proteins and the concentration of NPs, both determined by measuring their respective fluorescence intensities.

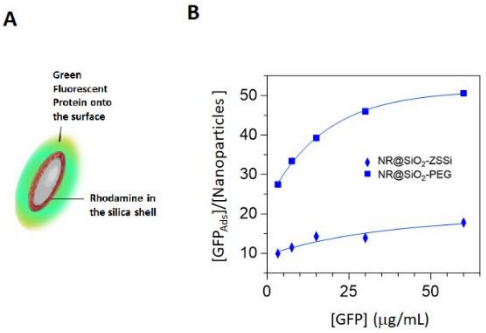

Fig. 8 A) Schematic diagram of the experiment carried out to measure protein adsorption. B) GFP adsorbed standardised by the quantity of NPs as a function of GFP introduced for NRs functionalised with PEG chains (NR@SiO2-PEG, blue squares) or with sulfobetaine molecules (NR@SiO2-ZSSi, blue diamonds). Solid lines are only a guide for the eye.

Surface functionalisation by zwitterionic sulfobetaine molecules was found to be much more effective in limiting protein adsorption. The quantity of proteins adsorbed is almost three times greater in the case of NPs functionalised by PEG chains, at all the protein concentrations studied. This greater efficiency of the sulfobetaine molecules in reducing the adsorption of the GFP is due to the greater stability of the NP hydration layer. Clearly, the water molecules interact more strongly with the surface by electrostatic interactions, in the case of sulfobetaine molecules, than by hydrogen bonding, in the case of PEG chains. They can therefore be more easily displaced from the surface, resulting in greater protein adsorption. Indeed, protein adsorption is an enthalpically unfavourable process, but the displacement of water molecules and counter ions during the pairing of the charged sites of the proteins with the surface charges provides a favourable entropic contribution. If this entropic contribution is sufficiently large to counterbalance the enthalpy of adsorption, then the free enthalpy of the protein adsorption process is negative and protein adsorption is spontaneous[61]. These results, combined with those of other studies highlighting intrinsic defects in PEG, such as its structural instability and immunogenicity[62], confirm that functionalization of the NPs surface by zwitterionic molecules is preferable to limit protein adsorption.

4. Conclusions

In summary, the two-step synthesis procedure studied produces magnetite NRs with a controlled shape and a high aspect ratio. The influence of the [PEI]/[Iron] ratio on the size of the akaganeite NRs obtained in the first step is predominant in the iron concentration range studied. The use of PEI also makes it possible to limit the polydispersity of the synthesised NPs to some extent. The reduction in the second step, using oleylamine as a solvent and reducing agent, effectively converts akaganeite to magnetite without losing the anisotropic shape of the NRs. The use of a [PEI]/[Iron] ratio = 1000 for an iron concentration of 0.1 mol/L allowed us to obtain magnetite NRs with a suitable size for the envisioned biomedical applications. Powder XRD, XANES and HR-TEM analyses confirmed that the NRs were single-crystal magnetite NPs. The magnetometry study revealed a relatively modest saturation magnetisation compared to bulk magnetite, counterbalanced by a much greater coercivity than for spherical NPs. These two characteristics underline the importance of shape anisotropy on magnetic properties.

A coating with silica enabled the surface of the magnetite NRs to be functionalised with either PEG chains or zwitterionic sulfobetaine molecules. The DLS study indicated that the dispersions obtained were stable, even in cell culture medium, for which no significant hydrodynamic size increase was observed. The zetametry study revealed an unusual behaviour for sulfobetaine-functionalised NRs, with an almost constant zeta potential over the entire studied pH range.

Surface functionalisation with these zwitterionic molecules reduces non-specific protein adsorption by a factor of around three compared to the functionalisation with PEG chains. This study therefore confirms the advantage of surface functionalization with zwitterionic groups in limiting protein adsorption, due to a more stable hydration layer with water molecules more strongly bound to the surface by electrostatic interactions.

Such magnetic NRs, characterised in particular by their high colloidal stability and their low non-specific adsorption of proteins, are promising candidates for future biomedical applications. Their anisotropic shape could be the key to giving them specific properties, different from their spherical counterparts, for diagnostic or therapeutic applications.

CRediT authorship contribution statement

S. El Mousli: Formal analysis, Investigation, Writing - Original Draft, Visualization. **Y. Dorant:** Formal analysis, Investigation. **E. Bertuit:** Formal analysis, Investigation. **E. Secret:** Conceptualization, Methodology, Validation, Writing - Review & Editing, Visualization, Supervision, Funding acquisition. **J.-M. Siaugue:** Conceptualization, Methodology, Validation, Writing - Review & Editing, Visualization, Supervision, Funding acquisition.

Declaration of competing interest

The authors declare that they have no known competing financial interests or personal relationships that could have appeared to influence the work reported in this paper.

Acknowledgements

We acknowledge SOLEIL for provision of synchrotron radiation facilities and we would like to thank Juliette Sirieix-Plénet and Anne-Laure Rollet for their assistance in XANES measurements and Valérie Briois for assistance in using beamline ROCK. We are thankful to David Montero for his assistance in SEM imaging, to David Hrabovsky at the MPBT (Physical Measurements at Low Temperatures) platform of Sorbonne Université for his assistance with magnetism measurements, to Aude Michel-Tourgis and Delphine Talbot for their help during total iron concentration measurements by AAS.

Data availability

Data will be made available on request.

References

[1] V. F. Cardoso, A. Francesko, C. Ribeiro, M. Bañobre-López, P. Martins, and S. Lanceros-Mendez, 'Advances in Magnetic Nanoparticles for Biomedical Applications', *Advanced Healthcare Materials*, vol. 7, no. 5, p. 1700845, Mar. 2018, doi: 10.1002/adhm.201700845.

[2] M. Tadic, S. Kralj, Y. Lalatonne, and L. Motte, 'Iron oxide nanochains coated with silica: Synthesis, surface effects and magnetic properties', *Applied Surface Science*, vol. 476, pp. 641–646, May 2019, doi: 10.1016/j.apsusc.2019.01.098.

[3] S. Shukla *et al.*, 'The Impact of Aspect Ratio on the Biodistribution and Tumor Homing of Rigid Soft-Matter Nanorods', *Adv. Healthcare Mater.*, vol. 4, no. 6, pp. 874–882, Apr. 2015, doi: 10.1002/adhm.201400641.

[4] J. Park *et al.*, 'Systematic Surface Engineering of Magnetic Nanoworms for In vivo Tumor Targeting', *Small*, vol. 5, no. 6, pp. 694–700, Mar. 2009, doi: 10.1002/smll.200801789.

[5] R. Agarwal *et al.*, 'Effect of Shape, Size, and Aspect Ratio on Nanoparticle Penetration and Distribution inside Solid Tissues Using 3D Spheroid Models', *Adv. Healthcare Mater.*, vol. 4, no. 15, pp. 2269–2280, Oct. 2015, doi: 10.1002/adhm.201500441.

[6] P. Kolhar *et al.*, 'Using shape effects to target antibody-coated nanoparticles to lung and brain endothelium', *Proc. Natl. Acad. Sci. U.S.A.*, vol. 110, no. 26, pp. 10753–10758, Jun. 2013, doi: 10.1073/pnas.1308345110.

[7] M. Tadic, J. Lazovic, M. Panjan, and S. Kralj, 'Hierarchical iron oxide nanocomposite: Bundle-like morphology, magnetic properties and potential biomedical application', *Ceramics International*, vol. 48, no. 11, pp. 16015–16022, Jun. 2022, doi: 10.1016/j.ceramint.2022.02.145.

[8] R. Madathiparambil Visalakshan *et al.*, 'The Influence of Nanoparticle Shape on Protein Corona Formation', *Small*, vol. 16, no. 25, p. 2000285, Jun. 2020, doi: 10.1002/smll.202000285.

[9] R. García-Álvarez, M. Hadjidemetriou, A. Sánchez-Iglesias, L. M. Liz-Marzán, and K. Kostarelos, '*In vivo* formation of protein corona on gold nanoparticles. The effect of their size and shape', *Nanoscale*, vol. 10, no. 3, pp. 1256–1264, 2018, doi: 10.1039/C7NR08322J.
[10] Z. Ma, J. Bai, Y. Wang, and X. Jiang, 'Impact of Shape and Pore Size of Mesoporous Silica Nanoparticles on Serum Protein Adsorption and RBCs Hemolysis', *ACS Appl. Mater. Interfaces*, vol. 6, no. 4, pp. 2431–2438, Feb. 2014, doi: 10.1021/am404860q.
[11] M. C. DeBrosse, K. K. Comfort, E. A. Untener, D. A. Comfort, and S. M. Hussain, 'High aspect ratio gold nanorods displayed augmented cellular internalization and surface chemistry mediated cytotoxicity', *Materials Science and Engineering: C*, vol. 33, no. 7, pp. 4094–4100, Oct. 2013, doi: 10.1016/j.msec.2013.05.056.
[12] L. Lacerda *et al.*, 'How do functionalized carbon nanotubes land on, bind to and pierce through model and plasma membranes', *Nanoscale*, vol. 5, no. 21, p. 10242, 2013, doi: 10.1039/c3nr03184e.
[13] L. Lacerda *et al.*, 'Translocation mechanisms of chemically functionalised carbon nanotubes across plasma membranes', *Biomaterials*, vol. 33, no. 11, pp. 3334–3343, Apr. 2012, doi: 10.1016/j.biomaterials.2012.01.024.
[14] A.-L. Papa, L. Dumont, D. Vandroux, and N. Millot, 'Titanate nanotubes: towards a novel and safer nanovector for cardiomyocytes*', *Nanotoxicology*, vol. 7, no. 6, pp. 1131–1142, Sep. 2012, doi: 10.3109/17435390.2012.710661.
[15] J. Mohapatra, A. Mitra, H. Tyagi, D. Bahadur, and M. Aslam, 'Iron oxide nanorods as high-performance magnetic resonance imaging contrast agents', *Nanoscale*, vol. 7, no. 20, pp. 9174–9184, 2015, doi: 10.1039/C5NR00055F.
[16] R. Das *et al.*, 'Tunable High Aspect Ratio Iron Oxide Nanorods for Enhanced Hyperthermia', *J. Phys. Chem. C*, vol. 120, no. 18, pp. 10086–10093, May 2016, doi: 10.1021/acs.jpcc.6b02006.
[17] J. Mohapatra *et al.*, 'Enhancing the magnetic and inductive heating properties of Fe_3O_4 nanoparticles via morphology control', *Nanotechnology*, vol. 31, no. 27, p. 275706, Apr. 2020, doi: 10.1088/1361-6528/ab84a3.
[18] S. Nath, C. Kaittanis, V. Ramachandran, N. S. Dalal, and J. M. Perez, 'Synthesis, Magnetic Characterization, and Sensing Applications of Novel Dextran-Coated Iron Oxide Nanorods', *Chem. Mater.*, vol. 21, no. 8, pp. 1761–1767, Apr. 2009, doi: 10.1021/cm8031863.
[19] W. Zhang, S. Jia, Q. Wu, J. Ran, S. Wu, and Y. Liu, 'Convenient synthesis of anisotropic Fe3O4 nanorods by reverse co-precipitation method with magnetic field-assisted', *Materials Letters*, vol. 65, no. 12, pp. 1973–1975, Jun. 2011, doi: 10.1016/j.matlet.2011.03.101.
[20] H. Sun, B. Chen, X. Jiao, Z. Jiang, Z. Qin, and D. Chen, 'Solvothermal Synthesis of Tunable Electroactive Magnetite Nanorods by Controlling the Side Reaction', *J. Phys. Chem. C*, vol. 116, no. 9, pp. 5476–5481, Mar. 2012, doi: 10.1021/jp211986a.
[21] L. Bao, W.-L. Low, J. Jiang, and J. Y. Ying, 'Colloidal synthesis of magnetic nanorods with tunable aspect ratios', *J. Mater. Chem.*, vol. 22, no. 15, p. 7117, 2012, doi: 10.1039/c2jm16401a.
[22] W. Wu *et al.*, 'Large-Scale and Controlled Synthesis of Iron Oxide Magnetic Short Nanotubes: Shape Evolution, Growth Mechanism, and Magnetic Properties', *J. Phys. Chem. C*, vol. 114, no. 39, pp. 16092–16103, Oct. 2010, doi: 10.1021/jp1010154.
[23] M. Tadic *et al.*, 'Surface-induced reversal of a phase transformation for the synthesis of ε-Fe2O3 nanoparticles with high coercivity', *Acta Materialia*, vol. 188, pp. 16–22, Apr. 2020, doi: 10.1016/j.actamat.2020.01.058.
[24] M. Tadic, M. Panjan, Y. Lalatone, I. Milosevic, B. V. Tadic, and J. Lazovic, 'Magnetic properties, phase evolution, hollow structure and biomedical application of hematite (α-Fe2O3) and QUAIPH', *Advanced Powder Technology*, vol. 33, no. 12, p. 103847, Dec. 2022, doi: 10.1016/j.apt.2022.103847.
[25] Y. Liu *et al.*, 'Facile Surface Functionalization of Hydrophobic Magnetic Nanoparticles', *Journal of the American Chemical Society*, vol. 136, no. 36, pp. 12552–12555, Sep. 2014, doi: 10.1021/ja5060324.

[26] Q. Li *et al.*, 'Zwitterionic Biomaterials', *Chem. Rev.*, vol. 122, no. 23, pp. 17073–17154, Dec. 2022, doi: 10.1021/acs.chemrev.2c00344.
[27] Z. G. Estephan, J. A. Jaber, and J. B. Schlenoff, 'Zwitterion-Stabilized Silica Nanoparticles: Toward Nonstick Nano', *Langmuir*, vol. 26, no. 22, pp. 16884–16889, Nov. 2010, doi: 10.1021/la103095d.
[28] H. Li, J. Han, and G. Liang, 'Phase Transfer of Hydrophobic Nanoparticles Using a Zwitterionic Sulfobetaine Siloxane Generates Highly Biocompatible and Compact Surfaces', *ACS Applied Nano Materials*, vol. 3, no. 2, pp. 1489–1496, Feb. 2020, doi: 10.1021/acsanm.9b02306.
[29] J. Mohapatra *et al.*, 'Enhancing the magnetic and inductive heating properties of Fe_3O_4 nanoparticles via morphology control', *Nanotechnology*, vol. 31, no. 27, p. 275706, Apr. 2020, doi: 10.1088/1361-6528/ab84a3.
[30] A. Orza, H. Wu, Y. Xu, Q. Lu, and H. Mao, 'One-Step Facile Synthesis of Highly Magnetic and Surface Functionalized Iron Oxide Nanorods for Biomarker-Targeted Applications', *ACS Applied Materials & Interfaces*, vol. 9, no. 24, pp. 20719–20727, Jun. 2017, doi: 10.1021/acsami.7b02575.
[31] L.-Y. Chen, Y.-T. Yin, C.-H. Chen, and J.-W. Chiou, 'Influence of Polyethyleneimine and Ammonium on the Growth of ZnO Nanowires by Hydrothermal Method', *J. Phys. Chem. C*, vol. 115, no. 43, pp. 20913–20919, Nov. 2011, doi: 10.1021/jp2056199.
[32] W. Xu *et al.*, 'Chemical Transformation of Colloidal Nanostructures with Morphological Preservation by Surface-Protection with Capping Ligands', *Nano Letters*, vol. 17, no. 4, pp. 2713–2718, Apr. 2017, doi: 10.1021/acs.nanolett.7b00758.
[33] H. Wu, D. Lee, L. T. Tufa, J. Kim, and J. Lee, 'Synthesis Mechanism of Magnetite Nanorods Containing Ordered Mesocages', *Chemistry of Materials*, p. acs.chemmater.9b00256, Mar. 2019, doi: 10.1021/acs.chemmater.9b00256.
[34] E. Amstad *et al.*, 'Influence of Electronegative Substituents on the Binding Affinity of Catechol-Derived Anchors to Fe_3O_4 Nanoparticles', *J. Phys. Chem. C*, vol. 115, no. 3, pp. 683–691, Jan. 2011, doi: 10.1021/jp1109306.
[35] E. Amstad, T. Gillich, I. Bilecka, M. Textor, and E. Reimhult, 'Ultrastable Iron Oxide Nanoparticle Colloidal Suspensions Using Dispersants with Catechol-Derived Anchor Groups', *Nano Lett.*, vol. 9, no. 12, pp. 4042–4048, Dec. 2009, doi: 10.1021/nl902212q.
[36] V. Maurice, T. Georgelin, J.-M. Siaugue, and V. Cabuil, 'Synthesis and characterization of functionalized core–shell γFe2O3–SiO2 nanoparticles', *Journal of Magnetism and Magnetic Materials*, vol. 321, no. 10, pp. 1408–1413, May 2009, doi: 10.1016/j.jmmm.2009.02.051.
[37] T. Georgelin, S. Bombard, J. Siaugue, and V. Cabuil, 'Nanoparticle-Mediated Delivery of Bleomycin', *Angewandte Chemie-International Edition*, vol. 49, no. 47, pp. 8897–8901, 2010, doi: 10.1002/anie.201003316.
[38] W. Stöber, A. Fink, and E. Bohn, 'Controlled growth of monodisperse silica spheres in the micron size range', *Journal of Colloid and Interface Science*, vol. 26, no. 1, pp. 62–69, Jan. 1968, doi: 10.1016/0021-9797(68)90272-5.
[39] H. Schöneborn *et al.*, 'Novel Tools towards Magnetic Guidance of Neurite Growth: (I) Guidance of Magnetic Nanoparticles into Neurite Extensions of Induced Human Neurons and In Vitro Functionalization with RAS Regulating Proteins', *Journal of Functional Biomaterials*, vol. 10, no. 3, p. 32, Jul. 2019, doi: 10.3390/jfb10030032.
[40] J. Tang, M. Myers, K. A. Bosnick, and L. E. Brus, 'Magnetite Fe_3O_4 Nanocrystals: Spectroscopic Observation of Aqueous Oxidation Kinetics', *J. Phys. Chem. B*, vol. 107, no. 30, pp. 7501–7506, Jul. 2003, doi: 10.1021/jp027048e.
[41] S. Link, M. B. Mohamed, and M. A. El-Sayed, 'Simulation of the Optical Absorption Spectra of Gold Nanorods as a Function of Their Aspect Ratio and the Effect of the Medium Dielectric Constant', *J. Phys. Chem. B*, vol. 103, no. 16, pp. 3073–3077, Apr. 1999, doi: 10.1021/jp990183f.
[42] W. F. J. Fontijn, P. J. Van Der Zaag, M. A. C. Devillers, V. A. M. Brabers, and R. Metselaar, 'Optical and magneto-optical polar Kerr spectra of Fe 3 O 4 and Mg 2 + - or Al 3 + -substituted

Fe 3 O 4', *Phys. Rev. B*, vol. 56, no. 9, pp. 5432–5442, Sep. 1997, doi: 10.1103/PhysRevB.56.5432.
[43] K. Voleník, M. Seberíni, and J. Neid, 'A Mössbauer and X-ray diffraction study of nonstoichiometry in magnetite', *Czech J Phys*, vol. 25, no. 9, pp. 1063–1071, Sep. 1975, doi: 10.1007/BF01597585.
[44] S. Gomes, M. François, M. Abdelmoula, Ph. Refait, C. Pellissier, and O. Evrard, 'Characterization of magnetite in silico-aluminous fly ash by SEM, TEM, XRD, magnetic susceptibility, and Mössbauer spectroscopy', *Cement and Concrete Research*, vol. 29, no. 11, pp. 1705–1711, Nov. 1999, doi: 10.1016/S0008-8846(99)00133-7.
[45] J. Mohapatra, A. Mitra, D. Bahadur, and M. Aslam, 'Surface controlled synthesis of MFe_2O_4 (M = Mn, Fe, Co, Ni and Zn) nanoparticles and their magnetic characteristics', *CrystEngComm*, vol. 15, no. 3, pp. 524–532, 2013, doi: 10.1039/C2CE25957E.
[46] A. Mitra, J. Mohapatra, H. Sharma, S. S. Meena, and M. Aslam, 'Controlled synthesis and enhanced tunnelling magnetoresistance in oriented Fe_3O_4 nanorod assemblies', *Journal of Physics D: Applied Physics*, vol. 51, no. 8, p. 085002, Feb. 2018, doi: 10.1088/1361-6463/aaa697.
[47] J. Choi, S. J. Oh, H. Ju, and J. Cheon, 'Massive Fabrication of Free-Standing One-Dimensional Co/Pt Nanostructures and Modulation of Ferromagnetism via a Programmable Barcode Layer Effect', *Nano Lett.*, vol. 5, no. 11, pp. 2179–2183, Nov. 2005, doi: 10.1021/nl051190k.
[48] J. Wan, Y. Yao, and G. Tang, 'Controlled-synthesis, characterization, and magnetic properties of Fe3O4 nanostructures', *Appl. Phys. A*, vol. 89, no. 2, pp. 529–532, Aug. 2007, doi: 10.1007/s00339-007-4107-5.
[49] R. Aragón, P. M. Gehring, and S. M. Shapiro, 'Stoichiometry, percolation, and Verwey ordering in magnetite', *Phys. Rev. Lett.*, vol. 70, no. 11, pp. 1635–1638, Mar. 1993, doi: 10.1103/PhysRevLett.70.1635.
[50] T. Kim *et al.*, 'Giant thermal hysteresis in Verwey transition of single domain Fe3O4 nanoparticles', *Sci Rep*, vol. 8, no. 1, p. 5092, Mar. 2018, doi: 10.1038/s41598-018-23456-6.
[51] J. P. Shepherd, J. W. Koenitzer, R. Aragón, J. Spal/ek, and J. M. Honig, 'Heat capacity and entropy of nonstoichiometric magnetite $Fe_3(1-\delta)O_4$: The thermodynamic nature of the Verwey transition', *Phys. Rev. B*, vol. 43, no. 10, pp. 8461–8471, Apr. 1991, doi: 10.1103/PhysRevB.43.8461.
[52] A. Mitra, J. Mohapatra, S. S. Meena, C. V. Tomy, and M. Aslam, 'Verwey Transition in Ultrasmall-Sized Octahedral Fe_3O_4 Nanoparticles', *J. Phys. Chem. C*, vol. 118, no. 33, pp. 19356–19362, Aug. 2014, doi: 10.1021/jp501652e.
[53] N. Lee *et al.*, 'Water-Dispersible Ferrimagnetic Iron Oxide Nanocubes with Extremely High r_2 Relaxivity for Highly Sensitive in Vivo MRI of Tumors', *Nano Lett.*, vol. 12, no. 6, pp. 3127–3131, Jun. 2012, doi: 10.1021/nl3010308.
[54] J. G. Croissant, K. S. Butler, J. I. Zink, and C. J. Brinker, 'Synthetic amorphous silica nanoparticles: toxicity, biomedical and environmental implications', *Nat Rev Mater*, vol. 5, no. 12, pp. 886–909, Dec. 2020, doi: 10.1038/s41578-020-0230-0.
[55] M. Pfeiffer-Laplaud, D. Costa, F. Tielens, M.-P. Gaigeot, and M. Sulpizi, 'Bimodal Acidity at the Amorphous Silica/Water Interface', *J. Phys. Chem. C*, vol. 119, no. 49, pp. 27354–27362, Dec. 2015, doi: 10.1021/acs.jpcc.5b02854.
[56] J. B. Schlenoff, 'Zwitteration: Coating Surfaces with Zwitterionic Functionality to Reduce Nonspecific Adsorption', *Langmuir*, vol. 30, no. 32, pp. 9625–9636, Aug. 2014, doi: 10.1021/la500057j.
[57] P. Zhang, B. D. Ratner, A. S. Hoffman, and S. Jiang, 'Nonfouling Surfaces', in *Biomaterials Science*, Elsevier, 2020, pp. 507–513. doi: 10.1016/B978-0-12-816137-1.00034-9.
[58] Q. Wei *et al.*, 'Protein Interactions with Polymer Coatings and Biomaterials', *Angew. Chem. Int. Ed.*, vol. 53, no. 31, pp. 8004–8031, Jul. 2014, doi: 10.1002/anie.201400546.
[59] S. Chen, J. Zheng, L. Li, and S. Jiang, 'Strong Resistance of Phosphorylcholine Self-Assembled Monolayers to Protein Adsorption: Insights into Nonfouling Properties of Zwitterionic

Materials', *J. Am. Chem. Soc.*, vol. 127, no. 41, pp. 14473–14478, Oct. 2005, doi: 10.1021/ja054169u.
[60] Q. Shao and S. Jiang, 'Molecular Understanding and Design of Zwitterionic Materials', *Adv. Mater.*, vol. 27, no. 1, pp. 15–26, Jan. 2015, doi: 10.1002/adma.201404059.
[61] Z. G. Estephan, P. S. Schlenoff, and J. B. Schlenoff, 'Zwitteration As an Alternative to PEGylation', *Langmuir*, vol. 27, no. 11, pp. 6794–6800, Jun. 2011, doi: 10.1021/la200227b.
[62] R. S. Kane, P. Deschatelets, and G. M. Whitesides, 'Kosmotropes Form the Basis of Protein-Resistant Surfaces', *Langmuir*, vol. 19, no. 6, pp. 2388–2391, Mar. 2003, doi: 10.1021/la020737x.